Surface-sensitive measurement of dielectric screening via atom and electron manipulations

Daejin Eom,* Eonmi Seo, and Ja-Yong Koo†
Korea Research Institute of Standards and Science, Yuseong, Daejeon 34113, Republic of Korea
(Received 8 August 2016; revised manuscript received 7 October 2016; published 16 November 2016)

Dielectric screening is essential in determining semiconductor properties. Its assessment on the surface, however, is beyond the capability of conventional techniques due to their lack of surface sensitivity. Here we present the surface-sensitive measurement of the dielectric screening by using scanning tunneling microscopy and spectroscopy. Both single-atom and single-electron manipulations on the B δ-doped Si(111) surface unravel that the dielectric screening on this surface is much in excess of what the classical image-charge model predicts, which we ascribe to the strained bonds and the ionic character of the surface layers. Also, as an exemplary application of the measured screening parameters, we demonstrate determining the ionization state of a surface defect from the defect-induced band bending.

DOI: 10.1103/PhysRevB.94.195308

I. INTRODUCTION

Dielectric screening is essential in determining various semiconductor properties such as the effective Bohr radius, the impurity level, the scattering cross section, and/or the effective Coulomb energy [1–5]. Therefore, it has been assessed extensively by using, for example, optical and capacitance techniques. It is, however, still challenging to measure the dielectric response of the surface layers directly without relying on a theoretical model due to the lack of conventional techniques in surface sensitivity [6]. Because of this difficulty, the so-called image-charge or half-space dielectric model [7] is adopted as the nominal dielectric response on the surface in most practices [8–11] while ignoring surface-specific features like structural reconstruction. However, the chemical bonds at the surface are often strained or relaxed and, therefore, are more easily polarizable than the bulk bonds [12]. Also the surface states may have smaller gaps than the bulk one, significantly contributing to the polarizability at the surface [13]. Hence, it might be critical to measure the surface dielectric behavior directly by using the surface-sensitive technique, if any, rather than to adopt the model prediction. Once measured successfully, it can be utilized to assess other physical quantities on the surface like the ionization state of a surface defect [14,15].

We have investigated B δ-doped Si(111) surfaces with $\sqrt{3}\times\sqrt{3}$ reconstruction ($\sqrt{3}$ surfaces) by using scanning tunneling microscopy and spectroscopy (STM and STS) [16]. This $\sqrt{3}$ surface is of particular interest because its dangling bonds (DBs) are passivated by the B acceptors, resulting in an enhanced chemical resistivity compared to other bare Si surfaces [17]. Thus it is often used as the nondissociative platform for growing organic molecules or supramolecular layers [18–21]. This surface also provides an ideal δ-doped layer in Si for which the B atoms regularly distribute in the third layer from the top surface [17,22,23]. Hence it can be a potential candidate for implementing the atomic-scale memory [24] or acceptor-based, scalable, qubit system [25,26] on it. Here we show the surface-sensitive measurement of the dielectric screening on the $\sqrt{3}$ surface via atom and electron manipulations. To be specific, we generate a single-atom defect on the surface and vary its ionization state by a single-electron charge. We then probe the resulting modulation in the surface potential with atomic resolutions, which enables us to assess the in-plane dielectric constant and Debye length on the $\sqrt{3}$ surface. Also, as an exemplary application of the measured screening parameters, we demonstrate determining the ionization state of a surface defect from the defect-induced band bending (DIBB).

II. EXPERIMENT

Our experiments were carried out by using a low-temperature STM in an ultrahigh vacuum chamber, the base pressure of which was below 1×10^{-10} Torr. An (111)-oriented, B-doped, crystalline Si with the resistivity of ~0.01 Ω cm or B concentration of $\sim 8.5\times10^{18}$ cm^{-3} was cleaned *in situ* by repeated thermal flashes at ~1200 K. It was then cooled down to room temperature at the rate of ~2 K/s after the last flash. After that, it was quenched down to 4.8 K for the STM and STS measurements.

III. RESULTS

Shown in Fig. 1(a) is an STM topography of the $\sqrt{3}$ surface that results from a dense B population in the surface region of Si(111) [17,22,23]. Its structural model is illustrated in Fig. 1(d), for which the B atom occupies a third of the substitutional sites of the third layer (S_5 sites) and the topmost Si atoms (Si adatoms) are sitting directly above them (T_4 sites). Figure 1(b) shows a spatially averaged differential conductance (dI/dV) spectrum measured on the $\sqrt{3}$ surface by using the STS technique. It clearly reveals the energy gap of ~1.1 eV and evolves no energy state within the gap region [24]. We also verify that the Fermi level (E_F) is located near the valence-band maximum (VBM) because of the significant hole doping and the low-temperature environment [27]. The energy level (E) will be referenced to E_F hereafter. The pronounced spectral feature at $E\simeq1.8$ eV in Fig. 1(b) is the unoccupied surface states of the $\sqrt{3}$ surface at the K point whereas a broad feature around $E\simeq-1.2$ eV is the occupied surface resonance states [28,29]. Now we generate a point defect on

*d.eom@kriss.re.kr
†koojayon@kriss.re.kr

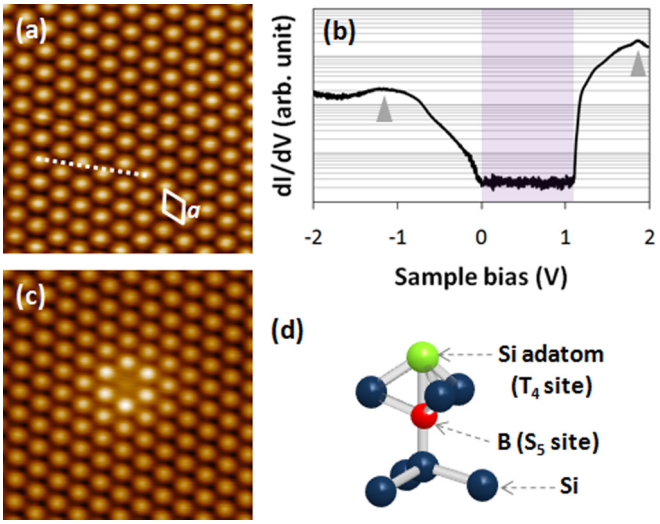

FIG. 1. (a) Topography of the $\sqrt{3}$ surface, which is taken with $V_{\text{sample}} = 2.5$ V and $I_t = 0.3$ nA. The lozenge indicates a surface unit cell with the lattice parameter a of 6.65 Å. (b) dI/dV spectrum averaged over the $\sqrt{3}$ surface in (a). It is displayed in a semilogarithmic scale. The shaded region is the band gap of silicon and the two arrows indicate the occupied and unoccupied surface states. (c) Topography of the same region as in (a) but imaged after applying V_{pulse} on the central adatom. It is taken with $V_{\text{sample}} = 2.5$ V and $I_t = 0.3$ nA. (d) Structural model of the $\sqrt{3}$ surface.

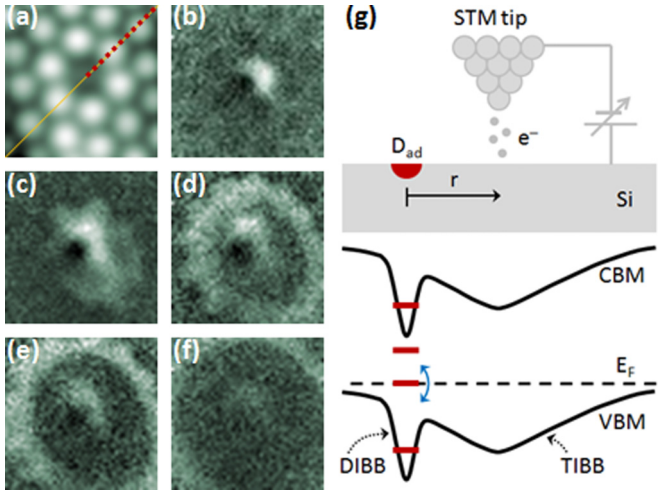

FIG. 2. (a) Topography of the $\sqrt{3}$ surface with a D_{ad} defect in the center. It is taken with $V_{\text{sample}} = 2.5$ V and $I_t = 0.3$ nA. (b)–(f) dI/dV maps taken over the region in (a). The sample biases are (b) −1.82 V, (c) −1.90 V, (d) −1.98 V, (e) −2.02 V, and (f) −2.08 V, respectively. (g) Schematic illustrating the charging mechanism in the D_{ad} defect. The charged defect causes the DIBB, which is superimposed by the TIBB centered at the distance r. A large TIBB makes one of the defect states (short line segments) cross E_F and be charged by an additional electron.

the $\sqrt{3}$ surface intentionally by placing an STM tip above a Si adatom and then applying a high-field bias pulse (V_{pulse}) on it with the feedback loop off [30]. Figure 1(c) displays a typical point defect generated on the clean $\sqrt{3}$ surface in Fig. 1(a). We will term this defect as the D_{ad} defect. We are not interested in the structural details of the D_{ad} defect in this paper but exploit it as the atomic-scale charge storage for the assessment of the dielectric screening on the $\sqrt{3}$ surface.

Since the charge amount in the D_{ad} defect is not known *a priori*, the Coulomb field emanating from it is not directly applicable for the quantitative assessment of the dielectric behavior of the $\sqrt{3}$ surface. It, however, is possible to vary its charge state by a definite amount, i.e., by a single-electron charge through the tip-induced band bending (TIBB) [31,32]. Such a charge state change would modify the electrostatic potential (ϕ) on the $\sqrt{3}$ surface proportionately, enabling us to measure its dielectric behavior. Figures 2(b)–2(f) display a typical example of the charging process in the D_{ad} defect through the TIBB. They are the dI/dV maps measured over the same region as the topography in Fig. 2(a) but with varying sample biases. Each image evolves a ringlike structure around the D_{ad} defect, which is indeed all the tip positions where the charging of the defect by single electron occurs at a given bias through the TIBB [10,33,34]: negative sample biases cause the band bend downward around the tip position as illustrated in Fig. 2(g). When the bias reaches a threshold value, an unoccupied gap state of the nearby defect crosses E_F and is charged by an electron. It then alters the electrostatic potential around the defect and causes an abrupt jump in the tunneling current (I) to larger magnitude at negative sample bias or, equivalently, a peak structure in the dI/dV spectrum. Since the band bending at the defect position is less effective with farther tip position from the defect, the charging process would occur at larger magnitude of negative sample bias, being consistent with the behavior in Figs. 2(b)–2(f).

We use the aforementioned current jump to quantify the surface potential change caused by the charging of the D_{ad} defect. The right curve in Fig. 3(a) shows a typical current spectrum measured at ∼7.4 Å away from the defect center. We divide it into three segments, i.e., blue, orange, and green ones, to highlight the current jump from blue to green through the orange one. If the charging event did not happen, the green curve would be a smooth extension of the blue one without the abrupt change as in the orange segment. In other words, the green curve would behave as displaced along the bias axis by $\Delta\phi$ so that it is linearly connected to the blue one as shown in the inset of Fig. 3(a). This current-preserving shift, $\Delta\phi$, along the bias axis is indeed a direct measure of the surface-potential change across the charging process in the D_{ad} defect because the identical potential difference between the tip and the sample surface would allow the same amount of tunneling current to flow between them. We have measured such voltage shifts at various positions along the dotted line in Fig. 2(a) and displayed them in Fig. 3(b). Once again, the shifting behavior in the interior of the defect is not our immediate concern in this study.

We now fit the measured $\Delta\phi$ outside the D_{ad} defect with a potential function to determine the screening parameters on the $\sqrt{3}$ surface. If an excess charge, q, is screened by the bound charges only, it produces the (ordinary) Coulomb potential [7]:

$$\phi(r) = \frac{1}{4\pi\kappa_s\varepsilon_0}\frac{q}{r} \tag{1}$$

where κ_s is the in-plane dielectric constant on the $\sqrt{3}$ surface and ε_0 is the vacuum permittivity. If it is screened

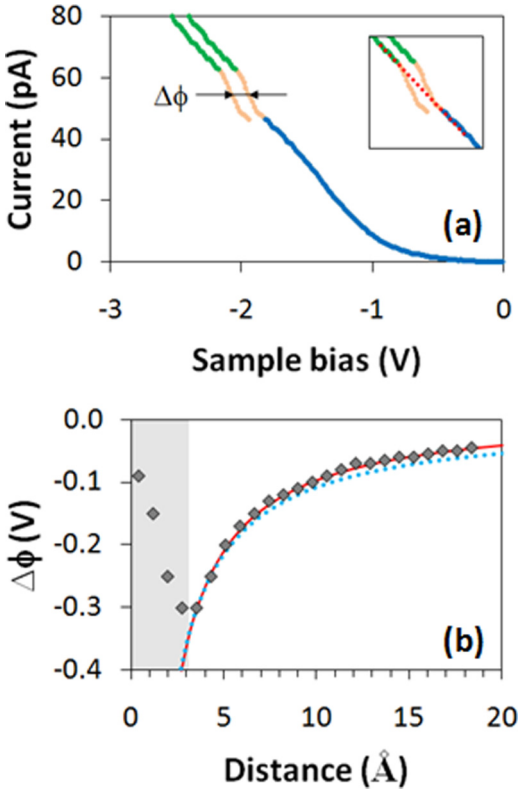

FIG. 3. (a) Current spectrum measured at ∼7.4 Å away from the center of the D_{ad} defect in Fig. 2(a). It is divided into three segments, i.e., blue, orange, and green ones. The displacement of green and orange segments along the bias axis by $\Delta\phi$ is displayed on the left side. Inset: The displaced green segment is linearly connected to the original blue one by adjusting $\Delta\phi$. (b) The diamond symbols represent the voltage shift $\Delta\phi$ measured at various positions along the dotted line in Fig. 2(a). The distance is referenced to the defect center. The shaded region is the interior of the D_{ad} defect. The dotted (solid) line is the fitting curve by the ordinary (screened) Coulomb potential with $\kappa_s = 13.3$ ($\kappa_s = 12.5$ and $\lambda_D = 56$ Å).

further by free charge carriers, it gives the screened Coulomb potential [35]:

$$\phi(r) = \frac{1}{4\pi\kappa_s\varepsilon_0}\frac{q}{r}e^{-r/\lambda_D} \tag{2}$$

where λ_D is the Debye length on the $\sqrt{3}$ surface. In the present case, the excess charge (q) is the sum of the initial charge (q_0) in the D_{ad} defect and its variation (Δq) by the TIBB, of which the latter is responsible for $\Delta\phi$ in Fig. 3(b). The dotted and solid curves in Fig. 3(b) are the best fits in the exterior of the defect ($r > 3.3$ Å) by Eqs. (1) and (2), respectively, with q replaced by Δq, i.e., the electron's charge ($-e$). The screened Coulomb potential with $\kappa_s = 12.5$ and $\lambda_D = 56$ Å fits to the data quite well (solid curve). The ordinary Coulomb potential with $\kappa_s = 13.3$ also closely fits to the data though slightly deviates at large distances (dotted curve). It is because the fitting range ($r < 20$ Å) is rather small compared to the Debye length.

Because the occupied surface states are far below the VBM, contributing a negligible amount of free carriers, the measured λ_D would be dictated by the bulk hole carriers. In this case the λ_D is written as [35]

$$\lambda_D = \left(\frac{\kappa_b\varepsilon_0 kT}{ne^2}\right)^{1/2} \tag{3}$$

where κ_b is the dielectric constant of bulk Si and n is its effective carrier density. If we use the known value for κ_b, i.e., 11.7 [36] along with the measured λ_D, we get $n \simeq 8.5 \times 10^{15}$ cm^{-3}. It is three orders of magnitude smaller than the nominal B concentration in our sample, i.e., $\sim 8.6 \times 10^{18}$ cm^{-3} [37]. Such discrepancy indeed originates from the temperature dependence of the carrier concentration [27]:

$$n = N_v e^{-(E_F - E_v)/kT} \tag{4}$$

where $N_v = 2[(m^* kT)/(2\pi\hbar^2)]^{3/2}$ is the effective density of states at the VBM, m^* is the effective hole mass, and E_v is the energy of the VBM. Since the N_v value at 4.8 K is two thousandths of that at 300 K, the temperature dependence of N_v would explain most of the above discrepancy.

As for the measured κ_s ($\geqslant 12.5$), it is much in excess of what the classical image-charge method predicts at the interface of two adjacent semi-infinite dielectric media [7], that is 6.35 [$= \frac{1}{2}(\kappa_b + 1)$] for our case. This enhanced κ_s implies that the surface region is more easily polarizable than the bulk. We ascribe it mainly to the strained bonds and the ionic character of the $\sqrt{3}$ surface.

(1) The covalent bonds between the topmost adatom and second layer Si atoms are severely distorted from the Si bulk structure [17,22,23], significantly weakening their strengths [see Fig. 1(d)]. Such strained and weak bonds would be more easily polarizable than the normal ones [12].

(2) The topmost adatom is positively charged whereas the underlying B atom at the S_5 site has the negative charge state [17]. Thus, not only the electronic polarization mechanism but the ionic one would work at the $\sqrt{3}$ surface [38,39], making the surface region more polarizable than the bulk. On the other hand, the surface state of the $\sqrt{3}$ surface has the bigger gap than the bulk one with the filled [empty] states far below the valence-band maximum (VBM) [above the conduction-band minimum (CBM)]. Hence their contribution to the surface polarization would be minor. The free charge carriers can also contribute to the static dielectric constant [7], that is, $\varepsilon = \varepsilon^{\text{bound}} + \varepsilon^{\text{free}}$ with

$$\varepsilon^{\text{free}} = -\frac{ne^2\tau^2}{m^*} = -n\mu^2 m^* \tag{5}$$

where τ and μ are the relaxation time and mobility of free carriers, respectively. If we use the above-determined n value at 4.8 K along with the hole mobility ($\leqslant 0.045$ m^2 V^{-1} s^{-1}) [40] and the hole mass ($\leqslant 0.49 m_0$) [27], we get $|\varepsilon^{\text{free}}/\varepsilon_0| < 1$. Thus the contribution of free carriers (holes) to the static dielectric constant is insignificant at 4.8 K. However, these free carriers may dominate the electric screening at room temperature due to the enhanced n by ~ 500 times, which makes $\varepsilon^{\text{free}}$ a large negative value and λ_D as small as 2.6 Å.

Since the screening parameters (κ_s and λ_D) are uncovered on the $\sqrt{3}$ surface, we can exploit them to determine the exact charge state of a surface defect, e.g., the D_{ad} defect from its DIBB. Figure 4(b) displays the dI/dV spectra probed in the clean region, i.e., along the line in Fig. 1(a), the spatial average

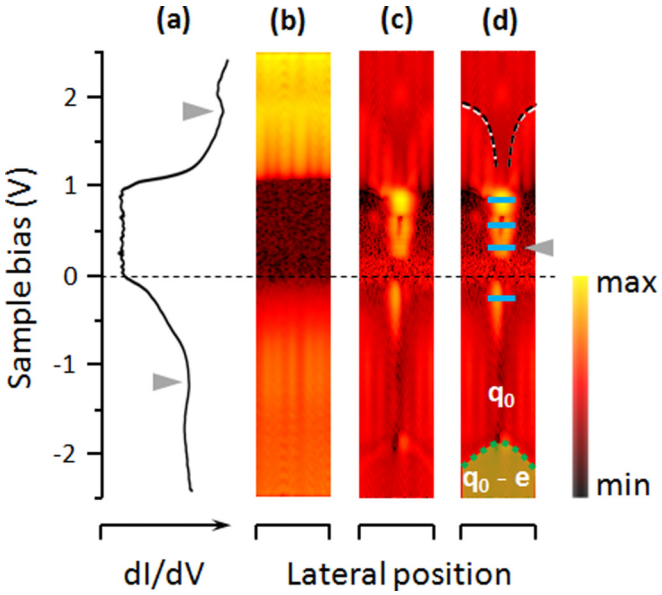

FIG. 4. (a) Spatially averaged dI/dV spectrum measured on the clean surface. The arrows indicate the unoccupied and occupied surface states. The horizontal axis has the logarithmic scale in arbitrary units. (b) Spatially resolved dI/dV spectra probed along the dotted line in Fig. 1(a). The magnitude of dI/dV is represented by a color code with the right-most scale bar. (c) Spatially resolved dI/dV spectra probed along the solid line in Fig. 2(a), being represented by the right-most scale bar. (d) A replica of (c) with several superimposed symbols. The short line segments indicate four defect states and the arrow indicates the lowest unoccupied defect level. The green dotted line at the bottom is the boundary where the charging of the D_{ad} defect takes place. Across the boundary, its charge state changes from q_0 to $q_0 - e$. The white and black lines in the upper part are the fitting curves by ordinary and screened Coulomb potentials, respectively, with $q_0 = +2e$. The lateral dimension in (b) to (d) is 31 Å.

of which is shown in Fig. 4(a). It exhibits a homogenous band profile along the horizontal axis with the characteristic spectral features like the VBM, the CBM, and the surface states. On the other hand, Figs. 4(c) and 4(d) are the spatially resolved dI/dV spectra across the D_{ad} defect, i.e., along the solid line in Fig. 2(a) and its replica, respectively. They display the defect-charging feature at $V_{sample} \leqslant -1.8$ V that we have discussed above. They also evolve four localized states as indicated by the short line segments in Fig. 4(d). Especially the state indicated by an arrow in Fig. 4(d) is responsible for the defect charging by the TIBB. The spectroscopic natures of those defect states, however, are not our concern in this study. Another distinct feature in Figs. 4(c) and 4(d) is the downward bending of the unoccupied surface states of the $\sqrt{3}$ surface near the D_{ad} defect. The CBM and VBM also exhibit similar bending profiles though they look more complicated than the unoccupied surface states due to the superposition of the defect states. Such a DIBB feature indicates that the D_{ad} defect is not neutral with respect to the clean surface but is positively charged. This charge (q_0) can be found by fitting the DIBB in Fig. 4(c) by either Eq. (1) or (2) with the predetermined screening parameters (κ_s and λ_D). The white and black curves in Fig. 4(d) are the best fit by Eqs. (1) and (2), respectively, which gives the initial defect charge q_0 of $+2e$.

IV. CONCLUSION

If we had adopted the surface dielectric constant from the image-charge model, the stationary charge of the D_{ad} defect would be $+1e$ and the charging amount causing $\Delta\phi$ in Fig. 3(b) would be $-0.5e$. This unphysical result underscores the importance of the actual assessment of the surface dielectric behavior beyond the model for the correct quantification of the defect charge on the semiconductor surfaces. Our surface-sensitive measurements of dielectric screening via atom and electron manipulations would be applicable to other semiconductor surfaces or van der Waals materials.

ACKNOWLEDGMENT

This work was supported by the basic Research and Development program of the Korea Research Institute of Standards and Science.

[1] C. Kittel and A. H. Mitchell, Phys. Rev. **96**, 1488 (1954).
[2] T. C. McGill and R. Baron, Phys. Rev. B **11**, 5208 (1975).
[3] D. Long and J. Myers, Phys. Rev. **115**, 1107 (1959).
[4] T. H. Nguyen, G. Mahieu, M. Berthe, B. Grandidier, C. Delerue, D. Stievenard, and Ph. Ebert, Phys. Rev. Lett. **105**, 226404 (2010).
[5] E. Şaşıoğlu, C. Friedrich, and S. Blügel, Phys. Rev. Lett. **109**, 146401 (2012).
[6] L. J. Brillson, *Surfaces and Interfaces of Electronic Materials*, 1st ed. (Wiley, New York, 2012).
[7] J. D. Jackson, *Classical Electrodynamics*, 3rd ed. (Wiley, New York, 1999).
[8] Ph. Ebert, X. Chen, M. Heinrich, M. Simon, K. Urban, and M. G. Lagally, Phys. Rev. Lett. **76**, 2089 (1996).
[9] A. Laubsch, K. Urban, and Ph. Ebert, Phys. Rev. B **80**, 245314 (2009).
[10] D.-H. Lee and J. A. Gupta, Nano Lett. **11**, 2004 (2011).
[11] D. Gohlke, R. Mishra, O. D. Restrepo, D. Lee, W. Windl, and J. Gupta, Nano Lett. **13**, 2418 (2013).
[12] S. K. Tripathy, Opt. Mater. **46**, 240 (2015).
[13] L. Reining and R. Del Sole, Phys. Rev. B **38**, 12768 (1988).
[14] E. G. Seebauer and M. C. Kratzer, *Charged Semiconductor Defects: Structure, Thermodynamics and Diffusion*, 1st ed. (Springer-Verlag, London, 2009).
[15] J. Bourgoin and M. Lannoo, *Point Defects in Semiconductors II: Experimental Aspects*, 1st ed. (Springer-Verlag, Berlin, 1983).
[16] V. V. Korobtsov, V. G. Lifshits, and A. V. Zotov, Surf. Sci. **195**, 466 (1988).
[17] I.-W. Lyo, E. Kaxiras, and Ph. Avouris, Phys. Rev. Lett. **63**, 1261 (1989).
[18] Y. Makoudi, F. Palmino, M. Arab, E. Duverger, and F. Chérioux, J. Am. Chem. Soc. **130**, 6670 (2008).

[19] O. Guillermet, A. Mahmood, J. Yang, J. Echeverria, J. Jeannoutot, S. Gauthier, C. Joachim, F. Chérioux, and F. Palmino, Chem. Phys. Chem. **15**, 271 (2014).
[20] S. R. Wagner and P. Zhang, J. Phys. Chem. C **118**, 2194 (2008).
[21] K. Boukari, E. Duverger, L. Stauffer, and Ph. Sonnet, Phys. Chem. Chem. Phys. **16**, 12164 (2014).
[22] P. Bedrossian, R. D. Meade, K. Mortensen, D. M. Chen, J. A. Golovchenko, and D. Vanderbilt, Phys. Rev. Lett. **63**, 1257 (1989).
[23] R. L. Headrick, I. K. Robinson, E. Vlieg, and L. C. Feldman, Phys. Rev. Lett. **63**, 1253 (1989).
[24] D. Eom, C.-Y. Moon, and J.-Y. Koo, Nano Lett. **15**, 398 (2015).
[25] J. Salfi, M. Tong, S. Rogge, and D. Culcer, Nanotechnology **27**, 244001 (2016).
[26] J. I. Cirac and P. Zoller, Nature (London) **404**, 579 (2000).
[27] S. M. Sze, *Semiconductor Devices: Physics and Technology*, 2nd ed. (Wiley, New York, 2001).
[28] E. Kaxiras, K. C. Pandey, F. J. Himpsel, and R. M. Tromp, Phys. Rev. B **41**, 1262 (1990).
[29] T. M. Grehk, P. Mårtensson, and J. M. Nicholls, Phys. Rev. B **46**, 2357 (1992).
[30] The tip-to-sample distance is initially set by the imaging condition, i.e., $V_{\text{sample}} = 2.5$ V and $I_t = 0.3$ nA. Then it is reduced by $\sim$3.5 Å with the feedback loop off. After that, a short-lasting bias pulse is applied, the magnitude of which is 3 V and the duration of which is 0.3 s.
[31] R. M. Feenstra, Y. Dong, M. P. Semtsiv, and W. T. Masselink, Nanotechnology **18**, 044015 (2007).
[32] R. Dombrowski, C. Steinebach, C. Wittneven, M. Morgenstern, and R. Wiesendanger, Phys. Rev. B **59**, 8043 (1999).
[33] N. A. Pradhan, N. Liu, C. Silien, and W. Ho, Phys. Rev. Lett. **94**, 076801 (2005).
[34] K. Teichmann, M. Wenderoth, S. Loth, R. G. Ulbrich, J. K. Garleff, A. P. Wijnheijmer, and P. M. Koenraad, Phys. Rev. Lett. **101**, 076103 (2008).
[35] M. Krčmar, W. M. Saslow, and M. B. Weimer, Phys. Rev. B **61**, 13821 (2000).
[36] L. Viña and M. Cardona, Phys. Rev. B **29**, 6739 (1984).
[37] Only the B atoms in the bulk are taken into account because the ionized B atoms in the delta-doped layer (at the S_5 sites) are compensated by the opposite charges of Si adatoms at the T_4 sites and, therefore, generate a negligible amount of hole carriers in the valence band.
[38] C. Kittel, *Introduction to Solid State Physics*, 6th ed. (Wiley, Singapore, 1991).
[39] K. F. Young and H. P. R. Frederikse, J. Phys. Chem. Ref. Data **2**, 313 (1973).
[40] F. J. Morin and J. P. Maita, Phys. Rev. **96**, 28 (1954).